Monthly Notices
of the
ROYAL ASTRONOMICAL SOCIETY

Mon. Not. R. Astron. Soc. **409,** 582–590 (2010) doi:10.1111/j.1365-2966.2010.17324.x

Abundance analyses of helium-rich subluminous B stars

Naslim N.,[1⋆] C. S. Jeffery,[1⋆] A. Ahmad,[1] N. T. Behara[1,2] and T. Şahìn[1,3]

[1]*Armagh Observatory, College Hill, Armagh BT61 9DG*
[2]*Institut d'Astronomie et d'Astrophysique, Université Libre de Bruxelles, Brussels B-1050, Belgium*
[3]*Department of Astronomy and The W.J. McDonald Observatory, The University of Texas at Austin, Austin, TX 78712, USA*

Accepted 2010 July 7. Received 2010 July 2; in original form 2010 May 27

ABSTRACT

The connection between helium-rich hot subdwarfs of spectral types O and B (He-sdB) has been relatively unexplored since the latter were found in significant numbers in the 1980s. In order to explore this connection further, we have analysed the surface composition of six He-sdB stars, including LB 1766, LB 3229, SB 21 (= Ton-S 137 = BPS 29503−0009), BPS 22940−0009, BPS 29496−0010 and BPS 22956−0094. Opacity-sampled line-blanketed model atmospheres have been used to derive atmospheric properties and elemental abundances. All the stars are moderately metal poor compared with the Sun ([Fe/H] ≈ -0.5). Four stars are nitrogen rich, two of these are carbon rich and at least four appear to be neon rich. The data are insufficient to rule out binarity in any of the sample. The surface composition and locus of the N-rich He-sdBs are currently best explained by the merger of two helium white dwarfs, or possibly by the merger of a helium white dwarf with a post-sdB white dwarf. C-rich He-sdBs require further investigation.

Key words: stars: abundances – stars: chemically peculiar – stars: early-type – stars: evolution – subdwarfs.

1 INTRODUCTION

Subdwarf B stars are low-mass core-helium burning stars with extremely thin hydrogen envelopes. They behave as helium main-sequence stars of roughly half a solar mass. Their atmospheres are generally helium deficient; radiative levitation and gravitational settling combine to make helium sink below the hydrogen-rich surface (Heber 1986).

However, almost 5 per cent of the total subdwarf population comprise stars with helium-rich atmospheres (Green, Schmidt & Liebert 1986; Ahmad & Jeffery 2006). The optical spectra of these stars are characterized by strong neutral helium lines and weak He II lines; they exhibit a wide range of helium abundance and effective temperatures ($T_{\rm eff}$) similar to both sdB and sdO stars. They have been variously classified as sdOB, sdOC and sdOD (Green et al. 1986) stars, but more recently as He-sdB and He-sdO stars (Moehler et al. 1990; Ahmad & Jeffery 2004). The spectroscopic division concerns the relative strengths of He I 4471, He II 4541 and Hγ (itself a blend of H and He II). Roughly speaking, the division occurs for stars with $T_{\rm eff} \approx 38\,000$ K (Drilling et al. 2003).

In general, He-sdB stars have lower surface gravities (g) than normal hydrogen-rich sdB stars (Heber 2009) and have spectral characteristics intermediate between extreme helium (EHe) stars (Jeffery 1996) and He-sdO stars (Napiwotzki 2008).

Most He-sdB stars show strong nitrogen (N II and N III) lines in their optical spectrum; these are referred to as N rich by Drilling et al. (2003). A few *also* showing strong carbon (C II and C III) lines are labelled C rich.

The question posed by these stars is that of their evolutionary status. Do He-sdB and He-sdO stars form a single sequence? Why are there C-rich and N-rich stars? Why is there such a large range in hydrogen abundance? How are they related to other classes of evolved star, including normal sdB stars? Is there a connection with any of the extreme helium stars (Jeffery 2008a,b)?

Possible origins include: a late core flash of a single post-giant-branch helium star evolving toward the white dwarf sequence (Lanz et al. 2004; Miller Bertolami et al. 2008); the merger of two helium white dwarfs (Iben 1990; Saio & Jeffery 2000) and the merger of a helium white dwarf with a post-sdB star (Justham et al. 2010). All of these scenarios are likely to produce hot subdwarfs with He-rich and N-rich surfaces. The second has also been argued to lead to helium-poor 'normal' sdB stars. All predict evolution tracks that commence with shell helium ignition in a white dwarf. They take the star to a yellow giant on a thermal time-scale and then to the helium main sequence on a nuclear time-scale. The details of the tracks differ in respect of their initial conditions and the microphysics adopted. Whether carbon is exposed is not clear.

The goal is, if possible, to distinguish clearly the various types of observed He-sdB (and He-sdO) stars and to connect each to one of these diverse origins.

The surface abundances of elements other than hydrogen and helium are therefore important indicators of previous evolution.

⋆E-mail: nas@arm.ac.uk (NN); csj@arm.ac.uk (CSJ)

© 2010 The Authors. Journal compilation © 2010 RAS

Downloaded from https://academic.oup.com/mnras/article/409/2/582/1036794 by Akdeniz University user on 20 September 2021

However first it is necessary to establish in what ranges these abundances lie, and hence to identify whether distinct groups exist. The challenge is that the numbers of He-sdB and He-sdO stars bright enough for fine analysis has hitherto been small, and very few, so far, have been found to be spectroscopically similar. The first of our studies was of PG 1544+488, which surprisingly turned out to be a short-period binary containing two helium-rich sdB stars (Ahmad & Jeffery 2004). The second was for JL 87 (Ahmad et al. 2007), a relatively bright and only moderately helium-rich ($n_{\rm He}/n_{\rm H} \approx 0.4$) and carbon-rich subdwarf. Far-ultraviolet spectra of these, and of LB 1766, were previously analysed by Lanz et al. (2004), with quite different results to our own. Ahmad et al. (2007) demonstrated the importance of establishing $T_{\rm eff}$, $\log g$ and carbon abundances from optical spectra of He I lines, i.e. relatively unblended lines with well-understood broadening theory, *before* extracting abundances of subordinate species.

We are therefore systematically acquiring high-resolution high signal-to-noise ratio (S/N) optical spectroscopy of He-sdB stars. Section 2 describes the observations used in this paper. These data are used to carry out detailed abundance analyses, making use of the latest generation of fully line-blanketed model atmospheres for appropriate mixtures (Section 3). Section 4 presents the results for our programme stars, which are discussed in terms of the evolution models and analyses of related objects in Section 5.

2 OBSERVATIONS

Spectra of several hydrogen-deficient stars were obtained with the University College London Echelle Spectrograph on the Anglo-Australian Telescope (AAT) in 2005 August. These included a number of He-sdB stars, namely LB 1766, LB 3229, SB 21 (=Ton-S 137 = BPS 29503−0009), BPS 22940−0009, BPS 29496−0010 and BPS 22956−0094. An extract from the observing log is shown in Table 1, which also indicates the S/N of the combined spectra used here. University College London echelle spectrograph (UCLES) was configured with the 31.6 lines mm^{-1} grating, the EEV2 detector and a slit width of 1.09 mm. A central wavelength of 4340.02 Å gives complete spectral coverage between 3820 and 5200 Å, and a nominal resolution with this slit width $R \approx 32\,000$. Exposures were broken into 1800-s segments in order to minimize cosmic ray contamination.

A preliminary analysis of three of these stars (LB 1766, SB 21 and BPS 22940−0009) using the same data was given by Naslim et al. (2010). SB 21 was originally identified as an extremely helium-rich subdwarf (Hunger & Kudritzki 1980); Hunger et al. (1981) found this star to be comparable with the helium-rich hot subdwarfs, CPD−31°1701 and TON-S 103. Abundances for LB 1766 were previously obtained from a far-ultraviolet (FUV) spectrum (Lanz et al. 2004); experience has demonstrated that an analysis of the FUV spectrum alone can lead to systematic errors (Ahmad et al. 2007). Our AAT spectra show LB 1766 and SB 21 to be nearly identical. Note that the original analyses (Hunger & Kudritzki 1980; Lanz et al. 2004) suggest these two stars to be quite different; thus a detailed contemporary comparison is important.

BPS 22940−0009 and BPS 29496−0010 were identified as He-sdB stars and BPS 22956−0094 as an sdB star in the survey of Beers et al. (1992). Our spectra show BPS 22940−0009 and BPS 22956−0094 to be carbon-rich He-sdB stars with strong C II, C III, N II, N III and He I lines. In contrast, LB 1766, SB 21, BPS 29496−0010 and LB 3229 are carbon-poor He-sdB stars, but with strong N II, N III and He I lines.

Table 1. AAT/UCLES observing log.

Star UT (start)	Seeing (arcsec)	α (2000) δ $t_{\rm exp}$ (s)	 S/N	$m_{\rm V}$
BPS CS 22940−0009		20 30 20	−59 50 50	13.8
2005 08 26 09:25:40	1.4	1800	10	
2005 08 26 09:56:33	1.4	1800	10	
2005 08 26 10:27:29	1.4	1800	12	
2005 08 26 10:58:22	1.4	1800	10	
Mean			21	
LB 1766		04 59 19	−53 52 52	12.3
2005 08 26 17:22:30	2.0	1800	35	
2005 08 26 17:53:23	2.0	1800	35	
2005 08 29 16:00:55	1.7	1800	20	
2005 08 29 16:31:49	1.7	1800	20	
Mean			61	
BPS CS 22956−0094		22 16 56	−64 31 51	–
2005 08 27 11:42:19	1.5	1800	17	
2005 08 27 12:13:13	1.5	1800	13	
2005 08 27 12:44:07	1.5	1800	20	
Mean			28	
BPS CS 29496−0010		23 34 02	−28 51 38	14.7
2005 08 27 14:07:52	1.8	1800	10	
2005 08 27 14:38:46	1.8	1800	10	
2005 08 27 15:09:40	1.8	1800	10	
2005 08 27 15:40:37	1.5	1800	10	
2005 08 27 16:21:17	1.5	1800	10	
2005 08 27 16:52:10	1.5	1800	10	
2005 08 27 17:23:04	1.5	1800	10	
2005 08 27 17:54:36	1.5	1800	10	
Mean			25	
LB 3229 = JL 261		01 47 17	−51 33 39	13.6
2005 08 27 18:29:28	1.5	1800	17	
2005 08 27 19:00:23	1.5	1800	18	
Mean			25	
SB 21 = PHL 645 = Ton-S 137 = BPS CS 29503−0009				
		00 04 31	−24 26 18	13.9
2005 08 28 14:46:45	1.2	1800	20	
2005 08 28 15:17:39	1.2	1800	20	
2005 08 28 15:48:33	1.2	1800	20	
2005 08 28 16:19:27	1.2	1800	19	
2005 08 28 16:50:21	1.2	1800	18	
2005 08 28 17:21:15	1.2	1800	18	
2005 08 28 17:52:09	1.2	1800	15	
2005 08 28 18:24:53	1.4	1800	17	
Mean			52	

The observations were reduced using a combination of ECHOMOP routines (Mills, Webb & Clayton 2006) and BESPOKE échelle reduction software (Şahìn 2008). The sky-subtracted wavelength-calibrated spectrum was extracted to a 2D format with each order represented by a single row. Continuum normalization was achieved by smoothing the 2D spectrum to form a 2D envelope spectrum, and then dividing by said envelope to remove most of the échelle blaze function. The smoothing procedure was adjusted to ensure that strong lines (Balmer or He I 4471 for example) were avoided when producing the normalization function. Order merging was carried out using the same 2D envelope to provide the weights at each wavelength in each overlap interval. A final normalization step

Downloaded from https://academic.oup.com/mnras/article/409/2/582/1036794 by Akdeniz University user on 20 September 2021

was carried out in which the merged 1D spectrum was divided by a low-order polynomial fitted to a set of continuum points defined manually.

We found no radial velocity shifts amongst the repeat spectra of individual stars, but only the data for LB 1766 were spread over a significant time interval (3 d).

In order to obtain a spectrum with the highest possible S/N, all of the individual spectra for each object were merged together, weighted appropriately for the S/N in each spectrum. The combined spectra were velocity shifted to the rest frame.

In an iterative process, we successfully identified all of the significant absorption lines visible in the combined spectra. Where observations allow (e.g. LB 1766 and SB 21), all known permitted and forbidden lines of He I can be identified (cf. HD 144941; Underhill 1966; Harrison & Jeffery 1997; Beauchamp & Wesemael 1998). He II 4686 is present in all targets. Hydrogen Balmer lines are evident in BPS 22956−0094. He II 4541 and other He II Pickering lines are present in LB 3229 and BPS 29496−0010. In the remainder, an Hβ/He II 4859 blend is present; it is not obvious from Hγ or He II 4541 which is dominant. In addition to N II, III, the target spectra variously show lines due to C II, III, O II, Ne II, Mg II, Al III, Si III, IV and S III. Identification charts are given in Figs A1–A6 (in the online version of the paper – see Supporting Information).

3 PHYSICAL PARAMETERS OF He-sdBs

The goal was to measure atmospheric physical parameters $T_{\rm eff}$, $\log g$ and elemental abundances for each star. We adopted two methods to determine $T_{\rm eff}$ and $\log g$. In the first we used ionization equilibria of prominent ions to determine $T_{\rm eff}$ and the profiles of Stark-broadened He I lines to determine $\log g$. In the second we used the χ^2 minimization package SFIT (Ahmad & Jeffery 2003) to determine $T_{\rm eff}$ and $\log g$ simultaneously.

3.1 Model atmospheres, line formation and spectral synthesis

Grids of model atmospheres for hydrogen-deficient stars were calculated using the local thermodynamic equilibrium (LTE) line-blanketed code STERNE (Behara & Jeffery 2006) which uses Opacity Project data for the continuous opacities, and treats line blanketing through opacity sampling in a data base of some 10^8 atomic transitions. In this case, we adopted grids with 1/10 solar metallicity, relative helium abundances $n_{\rm He} = 0.50$, 0.70, 0.90, 0.95, 0.989 and 0.999 by number,[1] and assumed microturbulent velocities $v_{\rm t} = 5$ and 10 km s^{-1}.

The choice of the 1/10 solar metallicity grid was adopted primarily because we were unable to obtain satisfactory fits for solar abundance models. The average abundances of Si and Mg, which are unlikely to have been affected by evolution, are subsolar by $\approx$0.5 dex (see below).

Given a model atmosphere, the LTE radiative-transfer code SPECTRUM (Jeffery, Woolf & Pollacco 2001) may be used to compute (a) individual line profiles and equivalent widths for given abundances and $v_{\rm t}$, (b) synthetic spectra for given wavelength ranges given the same information, and (c) the abundances of ions from individual lines of given equivalent width and $v_{\rm t}$.

For all of the programme stars except BPS CS 22956−0094, the Balmer lines were either weak or undetectable. Consequently we initially assumed a helium abundance $n_{\rm He} = 0.999$ ($n_{\rm H} = 0.0$) and model atmospheres with $v_{\rm t} = 5$ km s^{-1} as a starting approximation.

3.2 Microturbulent velocity

Using approximate values for $T_{\rm eff}$ and $\log g$, we measured the microturbulent velocity from the equivalent widths of 17 N II lines in LB 1766 and SB 21. Nitrogen abundances were calculated for microturbulent velocities in the range $v_{\rm t} = 0(5)\,20$ km s^{-1} using SPECTRUM. The microturbulent velocity determined by minimizing the scatter in the nitrogen abundance was $v_{\rm t} = 10 \pm 4$ km s^{-1}. We used the measured value of $v_{\rm t}$ in subsequent formal solution calculations for the ionization equilibrium and abundance measurements. For the instrumental profile, we adopted a Gaussian with full width at half-maximum (FWHM) = 2 resolution elements, corresponding to 0.1 Å or $R \approx 45\,000$. Additional broadening was attributed to rotation broadening and measured as part of the SFIT solution.

3.3 Ionization equilibrium and He I fitting

Using model atmospheres with $v_{\rm t} = 10$ km s^{-1}, the ionization equilibrium was established by balancing the abundances determined from N II and N III lines in each star, as well as by fitting the equivalent width of He II 4686. Values of $T_{\rm eff}$ were determined for several fixed values of $\log g$. Ideally, all ionization equilibria and profile fits should converge at a single point in parameter space. In practice they rarely do, possibly because of departures from LTE, which become increasingly important at $T_{\rm eff} > 30\,000$ K especially in certain strong He I and He II lines, possibly because of errors in equivalent width measurement, atomic data or some other reason.

Similarly, for a series of fixed values of $T_{\rm eff}$, we determined the value of $\log g$ by finding the best-fitting theoretical profile for the He I lines 4471, 4388 and 4922 Å (Fig. 1). The non-diffuse line He I 4121 is blended with nearby lines, and so was excluded from our analysis.

The coincidence of He I profile fits and the ionization equilibria was used to determine the overall solution illustrated in Fig. 2. Since the He II 4686 and N II/III temperatures do not coincide, and since the systematics of these two diagnostics are not yet clear, we have chosen an unweighted mean to determine the ionization temperature. The error in this mean is given by the quadratic mean of the formal error in the He II 4686 temperature and the standard deviation in the N II/III temperature.

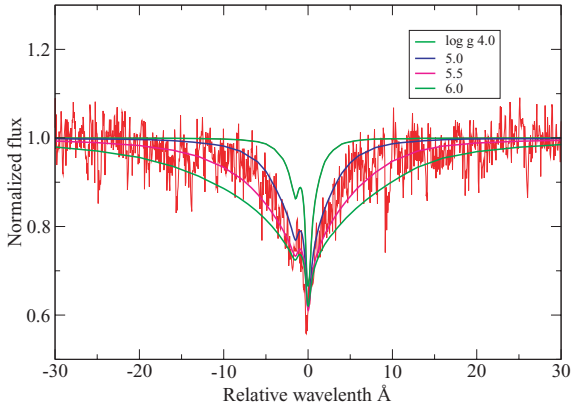


Figure 1. Theoretical model fits to He I 4471 in LB 3229 for model atmospheres with $n_{\rm He} = 0.989$, $T_{\rm eff} = 40\,000$ K and $\log g = 4.0(0.5)\,6.0$.

[1] Equivalent to $n_{\rm H} = 0.50$, 0.30, 0.10, 0.05, 0.01 and 0.0, respectively.

Downloaded from https://academic.oup.com/mnras/article/409/2/582/1036794 by Akdeniz University user on 20 September 2021

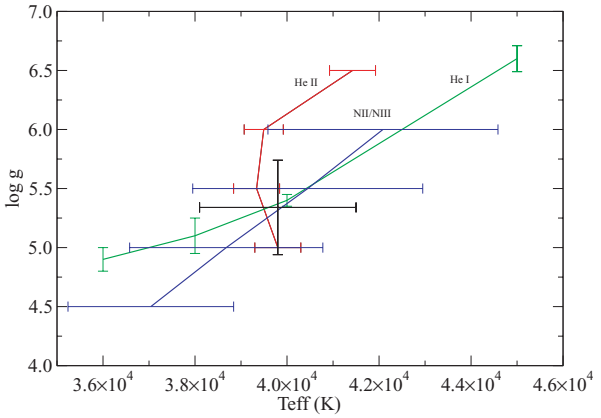


Figure 2. The loci of ionization equilibria for N II/N III and He II, the profile fits to He I lines and the adopted solution for LB 3229.

In practice, this procedure requires making a choice for the helium abundance. An estimate for $n_{\rm He}$ was obtained as described in the following section, and the grid helium abundance closest to that estimate was adopted.

3.4 χ^2 minimization

We measured the physical parameters $T_{\rm eff}$, $\log g$ and hydrogen abundance $n_{\rm H}$ using the package SFIT which finds the best-fitting solution within a grid of synthetic spectra. Although $n_{\rm He}$ is a parameter of the model grid, at high helium abundances it is actually a proxy for $n_{\rm H} = 1 - \Sigma_{i>1} n_i$; the He I lines are insensitive to abundance whilst, unusually for B stars, the Balmer lines vary strongly with abundance. SFIT works by fitting as many parameters and regions of spectrum simultaneously as the user chooses. Thus it measures $T_{\rm eff}$ from the relative strengths of helium lines, the ionization equilibria of all elements in the spectrum (e.g. He I/II, N II/III), $n_{\rm He}$ (or $n_{\rm H}$) from the strengths of hydrogen and helium lines and $\log g$ from profiles of Stark-broadened lines. In our analysis, spectral regions blueward of 4050 Å, where the broad wings of He I lines merge with one another, have been excluded because normalization is difficult.

The model grid used for the analysis of each star was a subset of a larger model grid in which $T_{\rm eff} = 32\,000$–$40\,000$, $50\,000$ K, $\log g = 4.00$–6.00, $v_{\rm t} = 10\,{\rm km\,s^{-1}}$ and $n_{\rm He} = 0.949, 0.989, 0.999$, except in the case of BPS 22956−0094, where $n_{\rm He} = 0.500, 0.699, 0.899$ was used. The grid spacings were $\delta T_{\rm eff} = 2000$ K and $\delta \log g = 0.5$. Since no grid was available for $n_{\rm He} = 0.949$ with $v_{\rm t} = 10\,{\rm km\,s^{-1}}$, we replaced this with a grid having $v_{\rm t} = 5\,{\rm km\,s^{-1}}$. The spectral fitting was done iteratively. In the initial iteration SFIT was run with three free parameters: $T_{\rm eff}$, $\log g$ and $n_{\rm He}$. The value of $n_{\rm He}$ was noted and fixed. In the final iteration $T_{\rm eff}$ and $\log g$ were solved simultaneously.

3.5 Atmospheric parameters

The atmospheric parameters of each star measured separately using SFIT and ionization equilibrium are given in Table 2. Both sets of results agree with one another to within the formal errors. In the case of LB 1766, $T_{\rm eff}$ is lower than in both previous studies, but close to that for SB 21, as would be indicated by the spectral similarity of these two stars. The model atmospheres are substantially improved, incorporating more appropriate line blanketing than in any previous studies, and this does account for significant shifts in $T_{\rm eff}$ in hydrogen-deficient atmospheres (Behara & Jeffery 2006).

Table 2. Atmospheric parameters.

Star	$T_{\rm eff}$ (K)	$\log g$	$n_{\rm He}$	$v_{\rm t}$ (km s^{-1})	$v \sin i$ (km s^{-1})	Source
BPS CS 22940−0009	33 700 ± 800	4.7 ± 0.2	0.993		4 ± 3	SFIT
	34 150 ± 1700	4.8 ± 0.2				Ionization equilibrium
	34 000	4.5	0.999	10		Adopted model
BPS CS 22956−0094	34 280 ± 800	5.63 ± 0.2	0.622		2 ± 1	SFIT
	34 100 ± 2000	5.52 ± 0.2				Ionization equilibrium
	34 000	5.5	0.699	5		Adopted model
SB 21	35 960 ± 500	5.4 ± 0.2	0.997		12 ± 2	SFIT
	36 500 ± 1500	5.6 ± 0.2				Ionization equilibrium
	36 000	5.5	0.999	10		Adopted model
	35 000	5.4				Hunger et al. (1981)
LB 1766	36 340 ± 500	5.19 ± 0.1	0.997		20 ± 3	SFIT
	35 600 ± 2100	5.15 ± 0.25				Ionization equilibrium
	36 000	5.0	0.999	10		Adopted model
	38 000 ± 500	5.5 ± 0.3				Ahmad & Jeffery (2003)
	40 000	6.3				Lanz et al. (2004)
BPS CS 29496−0010	39 150 ± 1000	5.65 ± 0.2	0.996		2 ± 1	SFIT
	39 770 ± 2300	5.8 ± 0.2				Ionization equilibrium
	40 000	5.5	0.999	10		Adopted model
LB 3229	40 000 ± 500	5.15 ± 0.2	0.988		8.5 ± 2	SFIT
	39 800 ± 1700	5.34 ± 0.4				Ionization equilibrium
	40 000	5.0	0.989	10		Adopted model

Downloaded from https://academic.oup.com/mnras/article/409/2/582/1036794 by Akdeniz University user on 20 September 2021

Table 3. Chemical abundances.

Star	Ref	H	He	C	N	O	Ne
LB 1766		<8.5	11.54	7.10 ± 0.23	8.29 ± 0.25	7.13 ± 0.30	8.62 ± 0.42
SB 21		<8.5	11.54	6.73 ± 0.18	8.24 ± 0.22	7.25 ± 0.27	8.49 ± 0.47
BPS CS 29496−0010		<8.5	11.54	6.88 ± 0.20	8.48 ± 0.24		
BPS CS 22940−0009		9.1 ± 0.2	11.54	8.94 ± 0.35	8.46 ± 0.22	7.11 ± 0.34	8.27 ± 0.45
LB 3229		9.3 ± 0.2	11.54	7.51 ± 0.27	8.66 ± 0.28		8.62 ± 0.38
BPS CS 22956−0094		11.1 ± 0.2	11.40	8.52 ± 0.35	8.33 ± 0.24		
LB 1766	1	9.53	11.53	7.06	8.77		
BX Cir	2	8.1	11.5	9.02	8.26	8.04	
V652 Her	3	9.38	11.54	7.14	8.93	7.54	8.38
JL 87	4	11.62	11.26	8.83	8.77	8.60	8.31
LS IV−14°116	5	11.95	11.23	8.47	8.23		
Sun	6, 7	12.00	[10.93]	8.52	7.92	8.83	[8.08]
Star	Ref	Mg	Al	Si	S		
LB 1766		7.17 ± 0.09	6.20 ± 0.18	7.03 ± 0.18	6.71 ± 0.20		
SB 21		7.24 ± 0.10	6.22 ± 0.10	6.98 ± 0.26	6.54 ± 0.13		
BPS CS 29496−0010		7.80 ± 0.19		7.05 ± 0.23	6.65 ± 0.15		
BPS CS 22940−0009		7.27 ± 0.18	6.12 ± 0.15	7.23 ± 0.24	6.45 ± 0.15		
LB 3229		8.21 ± 0.15		7.38 ± 0.22			
BPS CS 22956−0094		7.22 ± 0.13		6.82 ± 0.14	6.96 ± 0.10		
BX Cir	2	7.17	6.04	6.91	6.67		
V652 Her	3	7.76	6.49	7.49	7.44		
JL 87	4	7.36	6.28	7.22	6.88		
LS IV−14°116	5	6.95		6.63			
Sun	6	7.58	6.47	7.55	7.33		

References: 1 – Lanz et al. (2004); 2 – Drilling et al. (1998); 3 – Jeffery et al. (1999); 4 – Ahmad et al. (2007); 5 – Naslim et al. 2010; 6 – Grevesse & Sauval (1998); 7 – Dziembowski (1998) [the solar helium abundance is the asteroseismic value for the outer convection zone, the solar neon abundance is the meteoritic value; other solar abundances are for the solar photosphere].

3.6 Chemical abundances

Having measured $T_{\rm eff}$, $\log g$ and $n_{\rm He}$ for each star using two different methods, we chose the grid model atmosphere closest to these measured values (labelled 'Model' in Table 2). We measured equivalent widths of all C, N, O, Ne, Mg, Al, Si and S lines for which we had atomic data. SPECTRUM can compute a curve of growth for any given spectral line; given an equivalent width it will then return the elemental abundances for that line. Table A1 (in the online version of the paper – see Supporting Information) gives the adopted oscillator strengths (gf), measured equivalent widths and line abundances. Abundances are given in the form $\epsilon_i = \log n_i + c$ where $\log \Sigma_i a_i n_i = \log \Sigma_i a_i n_{i\odot} = 12.15$ and a_i are atomic weights. This form conserves values of ϵ_i for elements whose abundances do not change, even when the mean atomic mass of the mixture changes substantially.

Mean abundances for each element are reported in Table 3; in general, the errors represent the standard deviation of the line abundances about the mean. However, for Mg, Al and S, the error also includes the error on the equivalent width measurement estimated from the continuum noise. The errors in abundance $\delta\epsilon_i$ due to a representative systematic change in $\delta T_{\rm eff}$ or $\delta \log g$ are shown, for three stars, in Table A2 (in the online version of the paper – see Supporting Information).

The hydrogen abundances adopted previously were further refined by starting with a model spectrum for each star defined by the best model (Table 2) and abundances (Table 3), and by using SFIT to solve for the hydrogen abundance by fitting the Balmer lines only. In practice, only an upper limit of $n_{\rm H} < 0.001$ could be established for three stars, while the remaining three have the abundances shown in Table 3.

Table 3 compares the elemental abundances thus derived with those previously published for LB 1766, with those of more H-rich 'He-sdB' stars JL 87 and LS IV−14°116, two extreme helium stars V652 Her and BX Cir and the Sun. These will be discussed in the next section.

Theoretical spectra computed using the adopted grid atmosphere 'Model' (Table 2) and the adopted mean abundances (Table 3) are shown overplotted on the observed spectra in Figs A1–A6.

We note the following.

(1) Using silicon (five to eight lines), magnesium (one line), aluminium (two lines) and sulphur (two to three lines) as proxies for overall metallicity, the group is metal poor by $\approx 0.5 \pm 0.2$ dex compared with the Sun. We have not yet identified any iron lines in the optical spectra or analysed the FUSE spectrum of LB 1766.

(2) The majority are hydrogen deficient. The Balmer lines may be blended with weak He II lines. The hydrogen abundances are measured by χ^2 minimization in the model grid; errors are estimated. The exception is BPS CS 22956−0094.

(3) All stars are nitrogen rich ($+0.46 \pm 0.11$ dex) compared with the Sun, and significantly so ($\approx +1$ dex) after allowing for their low metallicity.

Downloaded from https://academic.oup.com/mnras/article/409/2/582/1036794 by Akdeniz University user on 20 September 2021

(4) After correcting for metallicity, the group ranges from very carbon rich (BPS 22940−0009 and BPS 22956−0094: ≈+0.8 dex) to very carbon poor (SB 21 and BPS CS 22496−0010: ≈−1.2 dex).

(5) In the two C-rich stars, the broad absorption at 4618 Å is not satisfactorily reproduced in the model. This anomalous line was first identified in H-deficient spectra by Klemola (1961), and discussed most recently by Leuenhagen, Hamann & Jeffery (1996).

(6) In all stars (four out of six) where it can be measured, neon appears to be significantly overabundant.

(7) The He I line fits are not uniformly satisfactory. In many cases, the observed line cores are substantially stronger than in the theoretical profiles. Here we suspect possible non-LTE (NLTE) effects. In a few cases, particularly where the S/N is low, one or both of the observed line wings lies below the theoretical profile. Here we suspect difficulties with the normalization – which has always been as conservative as possible.

4 EVOLUTIONARY STATUS OF He-sdBs

The evolutionary status of He-sdB and He-sdO stars has been discussed for some three decades. The location of these stars on and above the helium main-sequence points to low-mass helium stars which are either currently in a helium-core burning phase (the helium main sequence), or are approaching or leaving such a phase.

There has been a tendency to analyse and interpret He-sdO (Ströer et al. 2007; Napiwotzki 2008) and He-sdB stars (Lanz et al. 2004; Ahmad & Jeffery 2006) separately. This is partly due to the increasing importance of NLTE effects in sdO stars, and hence the adoption of different model atmospheres; a more self-consistent treatment of the two groups would be valuable. The apparent separation of the two groups in $T_{\rm eff}$–log g space (Fig. 3) may simply be a consequence of a significant range of $T_{\rm eff}$ within a group of stars having comparable luminosities. Nevertheless, it is clear that extremely helium-rich subdwarfs mark out a clear locus in this diagram, and that they are more luminous than the extended horizontal branch where hydrogen-rich sdB stars are generally found. In addition, there are a small number of cooler helium-rich stars, including V652 Her and BX Cir which may be closely linked to the helium-rich subdwarfs (He-sds).

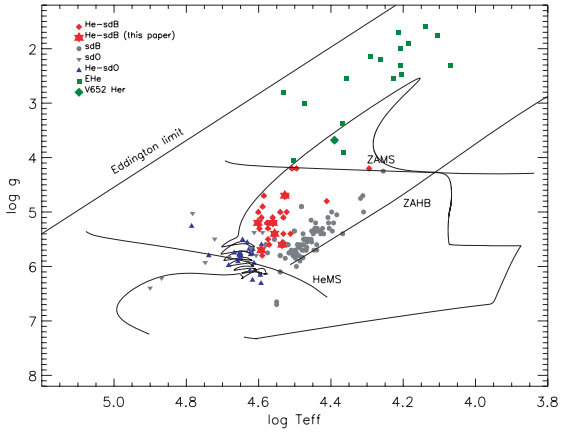


Figure 3. Comparison of hot helium-rich subdwarfs and extreme helium stars with the evolution of a helium white dwarf with $Z = 0.001$ following a late helium core flash (Miller Bertolami et al. 2008). The locations of normal sdBs (Edelmann et al. 2003), He-sdOs (Ströer et al. 2007), He-sdBs (Ahmad & Jeffery 2003), EHes (Pandey et al. 2006) and the stars discussed in this paper (N He-sdB) are identified separately (see key). For the latter, we adopt the SFIT results cited in Table 3.

The question of binarity is unresolved. The prototype He-sdB star PG 1544+488 is a binary consisting of two He-sdB stars (Ahmad, Jeffery & Fullerton 2004). Only one other binary He-sd, the double He-sdO star HE 0301−3039 (Lisker et al. 2004) has been reported. In such cases the extreme surface composition is a clear consequence of a close binary interaction, probably following a common-envelope phase, in which the entire hydrogen-rich envelope has been ejected. The question is then what differentiates the production of a He-rich subdwarf from a conventional H-rich sdB star in a close binary. Justham et al. (2010) propose a possible evolution following a double-core common-envelope phase involving intermediate-mass stars.

In the case of a close binary where envelope ejection exposes CNO-processed helium, the enhancement of nitrogen is easily explained by the conversion, and hence depletion, of carbon and oxygen in the CNO cycle. A similar abundance pattern is exhibited by the low-luminosity EHe star V652 Her (Jeffery, Hill & Heber 1999).

N-rich He-sds are less easy to explain in the absence of a binary companion. Equally problematic is C enrichment in either the single- or binary-star cases, since it requires the addition of carbon from 3α burning. The low-L EHe star BX Cir (Drilling, Jeffery & Heber 1998) provides a C-rich analogy to V652 Her. Neon is normally produced by α captures on to ^{14}N. Since both are plentiful in CNO-processed helium, a high-temperature episode in the formation of the He-sd might naturally give rise to an overabundance of neon.

Three evolutionary models have been proposed to address these questions for single He-sds.

4.1 The late hot flasher

Brown et al. (2001) proposed that single-star evolution with enhanced mass loss close to the tip of the red giant branch (RGB) will produce a star that suffers its helium-core flash late on the white dwarf cooling track. Since the flash occurs off-centre and when the outer layers are compact, flash-driven convection leads to mixing of the remnant H envelope with the helium core, and possibly also with some carbon from the He flash itself. The star initially expands to become a yellow giant, and then contracts towards the He main sequence as the helium-burning layers migrate to the centre of the star. Subsequent calculations have examined a number of variants of this model (Miller Bertolami et al. 2008) (Fig. 3). The result is either a N-rich or a C-rich He-sdB.

4.2 The double helium white dwarf merger

The merger of two helium white dwarfs has been proposed variously to account for both normal and helium-rich hot subdwarfs (Webbink 1984; Iben 1990; Tutukov & Yungel'Son 1990; Saio & Jeffery 2000). The progenitors are considered to be short-period systems from which most of the hydrogen and angular momentum has been ejected during a common-envelope phase. The surviving mass of hydrogen is very small relative to the total mixed mass (i.e. that of the disrupted white dwarf) $m_{\rm He}/m_{\rm mixed} \gtrsim 1.4 \times 10^{-4}/0.296$ (Iben & Tutukov 1986), where the hydrogen mass fraction would probably increase for lower mass white dwarfs.

Saio & Jeffery (2000) investigated the evolution of a helium white dwarf which rapidly accretes helium, i.e. as a result of merger with another helium white dwarf. Following off-centre helium ignition, the star expands to become a yellow giant, and then contracts as the helium shell burns inward through a series of mild flashes. The stable end state of such an evolution would most probably be a

Downloaded from https://academic.oup.com/mnras/article/409/2/582/1036794 by Akdeniz University user on 20 September 2021

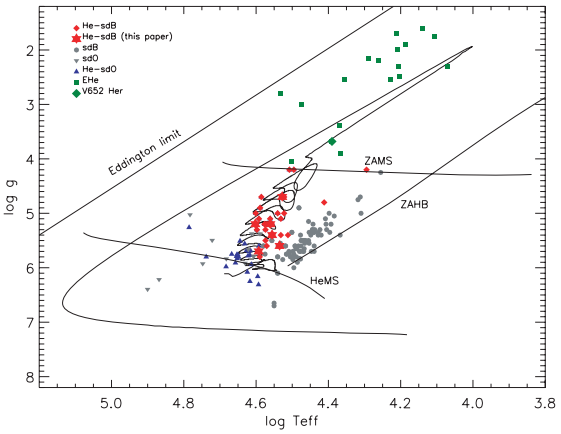


Figure 4. Comparison of hot helium-rich subdwarfs and extreme helium stars with the evolution of a $M_i = 0.3\,M_\odot$ helium white dwarf following the accretion of $0.2\,M_\odot$ helium to represent a double helium white dwarf merger (Saio & Jeffery 2000). Other symbols as for Fig. 3.

He-sdB or He-sdO star. The surface layers of such a star should be dominated by the nitrogen-enriched helium from the disrupted helium white dwarf. Saio & Jeffery (2000) found no evidence for surface carbon enrichment since each shell flash produces very little carbon and the subsequent flash-driven convection reaches the surface only after the first He-shell flash. The evolutionary track from one such model is shown in Fig. 4. Saio & Jeffery (2000) found that one such model would successfully account for the observed properties of the pulsating EHe star V652 Her, which must be in the shell-flashing phase.

4.3 The helium white dwarf plus hot subdwarf merger

Justham et al. (2010) have proposed a model in which a close binary containing a post-sdB star and a helium white dwarf merge. The post-sdB star is essentially a $0.46\,M_\odot$ hybrid white dwarf containing a small ($\approx 0.3\,M_\odot$) carbon–oxygen core and a helium envelope. The addition of fresh helium re-ignites the helium shell, and returns the star close to the helium main sequence with a helium-rich surface. Population synthesis calculations yield a $T_{\rm eff}$–$\log g$ distribution similar to that of the He-sdO stars of Ströer et al. (2007).

4.4 Evolutionary status of He-sdB stars

Comparison of the locus of He-sdB stars analysed here and by Ahmad & Jeffery (2003) with the evolutionary calculations discussed above (Figs 3 and 4) suggests that only the double helium white dwarf merger model successfully accounts for the distribution and surface composition of the N-rich He-sdBs. However, the evolution of both late hot flashers and white dwarf mergers is affected strongly by the metallicity, mass and envelope hydrogen content. Further exploration of the parameter space and of population statistics will be necessary to explain the origins of these evolved stars.

4.5 Surface-chemistry evolution in He-sdB stars

In all of the above evolutionary models, the initial surface composition might be assumed to be determined by the mean mass fractions obtained by combining several layers of stellar material.

For example, the surface of the double helium white dwarf merger would comprise any surviving hydrogen on the progenitor white dwarfs mixed with the helium core of the less massive component. The surface hydrogen to helium ratio (by mass) would then correspond roughly to the mass ratio of the hydrogen and helium layers in the latter, i.e. $\approx 5 \times 10^{-4}$ (see above, $\equiv 2 \times 10^{-3}$ by number). Meanwhile the CNO abundances would lie somewhere between a fully CNO-cycled mixture (i.e. carbon and oxygen converted to nitrogen) and a primordial mixture (i.e. carbon, nitrogen and oxygen scaled to the iron abundance), depending on the helium to hydrogen fraction. Additional carbon might be present if 3α burning occurs during the merger.

The surface of a late flasher will also be represented by CNO-processed helium, doped by whatever envelope hydrogen remained on the surface of the giant before hydrogen burning was extinguished. This may be anywhere in the ranges $n_{\rm H}/n_{\rm He} \approx 0.001$–$0.01$ (shallow mixing) or 10^{-5}–10^{-6} (deep mixing; Miller Bertolami et al. 2008). Carbon enrichment may occur if flash-driven convection can drive material to the surface after 3α ignition, and if the helium-envelope mass is small compared with the amount of carbon available for mixing (Cassisi & Vink 2003; Lanz et al. 2004).

The question is then what happens to this mixture as the star contracts towards the helium main sequence. It is well known that in a radiative stellar atmosphere having a sufficiently high surface gravity, an imbalance between the relative radiative and gravitational forces on individual ions leads to chemical separation of atomic species by the process of diffusion. Diffusion in subdwarf B stars, with $\log g > 5.5$ and $25\,000 \lesssim T_{\rm eff}/{\rm K} \lesssim 40\,000$ (Heber 1992), causes hydrogen to float and helium to sink so that observed helium abundances are typically in the range $0.001 < n_{\rm He}/n_{\rm H} < 0.01$.

At least two factors moderate the instantaneous conversion of a contracting He-sd into a normal H-rich sdB star. The first is that the diffusion time-scale is relatively long $\approx 10^5$ yr (Unglaub & Bues 2001, no stellar wind). The evolution time-scale essentially the thermal time-scale for the envelope and is $\approx 10^6$ yr for a merger involving a $0.2\,M_\odot$ white dwarf (Saio & Jeffery 2000), or $\approx 10^4$ yr for a late flasher with a $0.02\,M_\odot$ remnant envelope (Miller Bertolami et al. 2008).

The second factor is that a stellar wind acts to slow the diffusion process to give a time-scale $\approx 10^6$ yr (Unglaub 2005, 2008). Since winds in hot subdwarfs are radiatively driven, they are luminosity sensitive. Hence diffusion becomes more effective at low luminosity (high gravity). Helium depletion in the photosphere will accelerate as a star contracts towards the zero-age horizontal branch.

In the absence of winds, and if all He-sds were formed in the same way with identical envelope masses, one might expect to see a helium abundance gradient along the observed sequence, or at least to see the helium abundance drop as a helium-rich subdwarf contracts across the 'wind-line' – some critical luminosity below which diffusion becomes effective at reducing photospheric helium. The fact that the most hydrogen-rich 'He-sds' (i.e. BPS CS 22956−0094, JL 87, LS IV−14°116) are also those closest to the sdB domain might be important in this regard.

To explore such a hypothesis, Fig. 5 shows the distribution of hot subdwarfs as a function of helium abundance $\log y = \log (n_{\rm He}/n_{\rm H})$; the sample is exclusively that given in Figs 3 and 4. These observations indicate a substantial majority of normal sdB stars with negligible helium, a significant number of extremely He-rich stars on the pre-subdwarf cooling track and a continuum of hot subdwarfs with relatively high gravities and intermediate helium abundances ($-1 < \log y < +1$). In numerical terms, there are roughly 100 normal sdBs for every 10 helium-rich plus intermediate helium subdwarfs (Green et al. 1986), and 18 helium-rich He-sdBs for nine intermediate He-sdBs (Fig. 5); better statistics would be valuable.

Downloaded from https://academic.oup.com/mnras/article/409/2/582/1036794 by Akdeniz University user on 20 September 2021

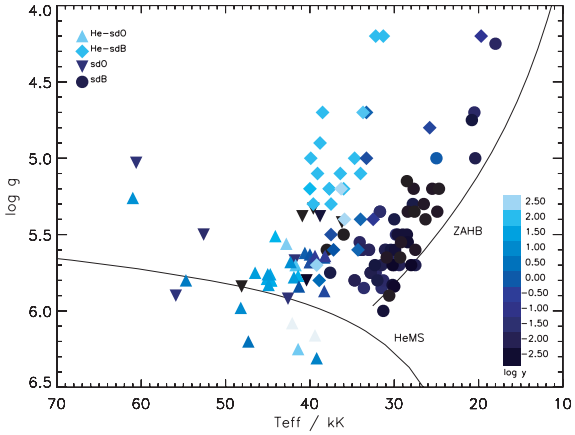


Figure 5. Distribution of helium abundance versus $T_{\rm eff}$ and $\log g$. The helium abundance $\log y = \log(n_{\rm He}/n_{\rm H})$ is indicated by colour (or grey-scale) as shown in the key. The data shown include the He-sdB, He-sdO, sdB and sdO stars from Figs 3 and 4.

Hot subdwarfs with intermediate helium abundances might then represent stars in which diffusion has started to operate, but in which some helium remains visible. The ratio of intermediate helium subdwarfs to normal subdwarfs should then be given approximately by the ratio of the diffusion time-scale ($\approx 10^6$ yr) to the sdB nuclear time-scale ($\approx 10^8$ yr) times the fraction of sdB stars formed through channels which involve a helium-rich progenitor ($\lesssim 0.5$), leading to a total of roughly one intermediate helium subdwarf in 100, slightly fewer than observed.

One problem with this argument, and there are many, is that helium-rich sdB stars may simply become helium-rich sdO stars on the helium main sequence and may *not* evolve into helium-poor sdB stars. A more detailed examination of surface abundances of other species, including iron, in several helium-rich hot subdwarfs will be necessary.

One observation, however, is instructive. Amongst the helium-rich subdwarfs studied by Ahmad & Jeffery (2006), Ströer et al. (2007) and ourselves, stars with intermediate helium abundances lie predominantly at the boundary between the He-poor and He-rich subdwarfs in the $\log g - T_{\rm eff}$ diagram. There are virtually no He-poor subdwarfs significantly above the horizontal branch (Fig. 5), i.e. with $T_{\rm eff} > 30\,000$ K and $\log g < 5.3$. This observation is supported by low-resolution classification surveys (Drilling et al. 2003; Winter et al. 2006). *Thus, if subdwarfs evolve on to either the helium main sequence or the extended horizontal branch by contracting from a more expanded configuration, then the only ones which are currently observed to be doing so are helium rich.*

5 CONCLUSION

As part of an extended study of the surface abundances of extremely helium-rich hot subdwarfs, high-resolution optical échelle spectra of the He-sdB stars LB 1766, SB 21, BPS CS 22940−0009, BPS CS 29496−001, BPS CS 22956−0094 and LB 3229 have been presented. Opacity-sampled line-blanketed model atmospheres have been used to derive atmospheric properties and surface abundances.

All the stars analysed are moderately metal poor compared with the Sun ([Fe/H] ≈ -0.5). LB 1766, SB 21, BPS CS 29496−001 and LB 3229 are nitrogen-rich He-sdBs, while BPS CS 22940−0009 and BPS CS 22956−0094 are carbon-rich He-sdBs. The former have a surface composition and *L*/*M* ratio comparable with the extreme helium star V652 Her, while the latter might be more directly compared with the extreme helium star BX Cir.

The evolutionary status of He-sdBs has been discussed in the context of (i) close binary star evolution, (ii) a late helium flash in a post-RGB star, (iii) the merger of two helium white dwarfs and (iv) the merger of a helium white dwarf with a post-sdB star. The surface composition and locus of single N-rich He-sdBs are currently best explained by the merger of two helium white dwarfs, although this may not necessarily be a unique solution. The merger of a helium white dwarf with a post-sdB white dwarf offers an interesting alternative. C-rich He-sdBs require further investigation; the origin of surface carbon is difficult to explain without mixing 3α products to the surface and so far, only the late flasher model seems capable of this. An overabundance of neon requires further explanation.

On the basis of any of these evolution tracks, the EHe stars V652 Her and BX Cir are likely to evolve to become He-sdB stars. He-sdB stars are likely to evolve to become He-sdO stars.

ACKNOWLEDGMENTS

This paper is based on observations obtained at the Anglo-Australian Telescope. It has made use of the SIMBAD data base, operated at CDS, Strasbourg, France. The Armagh Observatory is funded by direct grant from the Northern Ireland Department of Culture Arts and Leisure.

REFERENCES

Ahmad A., Jeffery C. S., 2003, A&A, 402, 335
Ahmad A., Jeffery C. S., 2004, Ap&SS, 291, 253
Ahmad A., Jeffery C. S., 2006, Baltic Astron., 15, 139
Ahmad A., Jeffery C. S., Fullerton A. W., 2004, A&A, 418, 275
Ahmad A., Behara N. T., Jeffery C. S., Sahin T., Woolf V. M., 2007, A&A, 465, 541
Beauchamp A., Wesemael F., 1998, ApJ, 496, 395
Beers T. C., Doinidis S. P., Griffin K. E., Preston G. W., Shectman S. A., 1992, AJ, 103, 267
Behara N. T., Jeffery C. S., 2006, A&A, 451, 643
Brown T. M., Sweigart A. V., Lanz T., Landsman W. B., Hubeny I., 2001, ApJ, 562, 368
Cassisi S., Vink J. S., 2003, in Piotto G., Meylan G., Djorgovski S. G., Riello M., eds, ASP Conf. Ser. Vol. 296, New Horizons in Globular Cluster Astronomy. Astron. Soc. Pac., San Francisco, p. 201
Drilling J. S., Jeffery C. S., Heber U., 1998, A&A, 329, 1019
Drilling J. S., Moehler S., Jeffery C. S., Heber U., Napiwotzki R., 2003, in Gray R. O., Corbally C. J., Philip A. G. D., eds, The Garrison Festschrift Spectral Classification of Hot Subdwarfs. Univ. Arizona Press, Tucson, p. 27
Dziembowski W. A., 1998, Space Sci. Rev., 85, 37
Edelmann H., Heber U., Hagen H., Lemke M., Dreizler S., Napiwotzki R., Engels D., 2003, A&A, 400, 939
Green R. F., Schmidt M., Liebert J., 1986, ApJS, 61, 305
Grevesse N., Sauval A. J., 1998, Space Sci. Rev., 85, 161
Harrison P. M., Jeffery C. S., 1997, A&A, 323, 177
Heber U., 1986, A&A, 155, 33
Heber U., 1992, in Heber U., Jeffery C. S., eds, Lecture Notes in Physics, Vol. 401, The Atmospheres of Early-Type Stars. Springer-Verlag, Berlin, p. 233
Heber U., 2009, ARA&A, 47, 211
Hunger K., Kudritzki R. P., 1980, A&A, 88, L4
Hunger K., Gruschinske J., Kudritzki R. P., Simon K. P., 1981, A&A, 95, 244
Iben I. J., 1990, ApJ, 353, 215

© 2010 The Authors. Journal compilation © 2010 RAS, MNRAS **409,** 582–590

Downloaded from https://academic.oup.com/mnras/article/409/2/582/1036794 by Akdeniz University user on 20 September 2021

Iben I., Jr, Tutukov A. V., 1986, ApJ, 311, 742
Jeffery C. S., 1996, in Jeffery C. S., Heber U., eds, ASP Conf. Ser. Vol. 96, Hydrogen Deficient Stars. Astron. Soc. Pac., San Francisco, p. 152
Jeffery C. S., 2008a, in Werner A., Rauch T., eds, ASP Conf. Ser. Vol. 391, Hydrogen-Deficient Stars. Astron. Soc. Pac., San Francisco, p. 3
Jeffery C. S., 2008b, Inf. Bull. Var. Stars, 5817, 1
Jeffery C. S., Hill P. W., Heber U., 1999, A&A, 346, 491
Jeffery C. S., Woolf V. M., Pollacco D. L., 2001, A&A, 376, 497
Justham S., Podsiadlowski P., Han Z., Wolf C., 2010, Ap&SS, in press
Klemola A. R., 1961, ApJ, 134, 130
Lanz T., Brown T. M., Sweigart A. V., Hubeny I., Landsman W. B., 2004, ApJ, 602, 342
Leuenhagen U., Hamann W.-R., Jeffery C. S., 1996, A&A, 312, 167
Lisker T., Heber U., Napiwotzki R., Christlieb N., Reimers D., Homeier D., 2004, Ap&SS, 291, 351
Miller Bertolami M. M., Althaus L. G., Unglaub K., Weiss A., 2008, A&A, 491, 253
Mills D., Webb J., Clayton W., 2006, Starlink User Note, 152
Moehler S., Richtler T., de Boer K. S., Dettmar R. J., Heber U., 1990, A&AS, 86, 53
Napiwotzki R., 2008, in Werner A., Rauch T., eds, ASP Conf. Ser. Vol. 391, Hydrogen-Deficient Stars. Astron. Soc. Pac., San Francisco, p. 257
Naslim N., Jeffery C. S., Ahmad A., Behara N., Şahın T., 2010, Ap&SS, in press
Naslim N., Jeffery C. S., Behara N. T., Hibbert A., 2010, MNRAS, submitted
Pandey G., Lambert D. L., Jeffery C. S., Rao N. K., 2006, ApJ, 638, 454
Şah'ın T., 2008, PhD thesis, Queens University, Belfast
Saio H., Jeffery C. S., 2000, MNRAS, 313, 671
Ströer A., Heber U., Lisker T., Napiwotzki R., Dreizler S., Christlieb N., Reimers D., 2007, A&A, 462, 269
Tutukov A. V., Yungel'Son L. R., 1990, Astron. Zh., 67, 109
Underhill A., 1966, The Early Type Stars. Reidel, Dordrecht
Unglaub K., 2005, in Koester D., Moehler S., eds, ASP Conf. Ser. Vol. 334, 14th European Workshop on White Dwarfs. Astron. Soc. Pac., San Francisco, p. 297
Unglaub K., 2008, A&A, 486, 923
Unglaub K., Bues I., 2001, A&A, 374, 570
Webbink R. F., 1984, ApJ, 277, 355
Winter C., Jeffery C. S., Ahmad A., Morgan D. R., 2006, Baltic Astron., 15, 69

SUPPORTING INFORMATION

Additional Supporting Information may be found in the online version of this article:

Table A1. Oscillator strength, measured equivalent width and derived elemental abundance for each line measured in the six programme stars.
Table A2. Abundance errors due to errors in $T_{\rm eff}$ and $\log g$.
Figure A1. The AAT spectrum of LB 1766.
Figure A2. The AAT spectrum of SB 21.
Figure A3. The AAT spectrum of LB 3229.
Figure A4. The AAT spectrum of BPS 22940−0009.
Figure A5. The AAT spectrum of BPS 22956−0094.
Figure A6. The AAT spectrum of BPS 29496−0010.

Please note: Wiley-Blackwell are not responsible for the content or functionality of any supporting materials supplied by the authors. Any queries (other than missing material) should be directed to the corresponding author for the article.

This paper has been typeset from a TEX/LATEX file prepared by the author.

Downloaded from https://academic.oup.com/mnras/article/409/2/582/1036794 by Akdeniz University user on 20 September 2021